Markov-Chain Formulation of Reaction-Diffusion Model and its Implications for Statistical Distribution of Interface Defects in Nanoscale Transistors

*Ahmad Ehteshamul Islam and **Muhammad Ashraful Alam

*Department of Materials Science and Engineering, University of Illinois, Urbana, IL 61801, USA.

**School of Electrical and Computer Engineering, Purdue University, West Lafayette, IN 47907-2035, USA.

Email: *aeislam@ieee.org; **alam@purdue.edu

Abstract

Continued scaling of nanoscale transistors leads to broad device-to-device fluctuation of parameters due to random dopant effects, channel length variation, interface trap generation, etc. In this paper, we obtain the statistics of negative bias temperature instability (NBTI)-induced interface defect generation in ultra-scaled MOSFET by Markov Chain Monte-Carlo (MCMC) solution of Reaction-Diffusion (R-D) model. Our results show that the interface defect generation at a particular stress time, i.e., $N_{IT}@t_{STS}$ in small transistors should follow a skew-normal distribution and that the generation and annealing of interface defects are strongly correlated. Next, we use a random percolative network to demonstrate (which is also consistent with previously published results in literature based on separate techniques) that the distribution of threshold voltage shift for single interface defect, i.e., $\Delta V_T@N_{IT}$ is exponential, with finite number of transistors having zero ΔV_T. Finally, we show that the statistics of $\Delta V_T@t_{STS}$ – based on the convolution of $N_{IT}@t_{STS}$ and $\Delta V_T@N_{IT}$ – is broadly consistent with the available experimental data in literature.

Keywords:

Reaction-Diffusion (R-D) model, Markov chain Monte-Carlo (MCMC), interface defect, statistics, skew normal distribution, exponential distribution, threshold voltage degradation.

1. Introduction

Defect-induced threshold voltage shift (ΔV_T) has been a reliability issue in metal-oxide-semiconductor (MOS) transistors since the 1970s. Such instability has been amplified in modern nanoscale MOS transistors due to the use of high-κ gate dielectric and also due to the presence of higher oxide electric field[1-8]. Therefore, time evolution of threshold voltage (a phenomenon, also known as Bias Temperature Instability or BTI) for every technology generation must be carefully and critically examined to ensure the long-term viability of an IC. For simplicity of such test and qualification, the BTI tests frequently use large-area test transistors with appropriate average threshold voltage shift $<\Delta V_T>$ at the end of product lifetime. However, dimension of modern transistors are so small that product qualification requires knowledge of ΔV_T statistics, in addition to $<\Delta V_T>$. For example, given the typical defect density of ~10^{12} cm^{-2}, a 45 nm SRAM memory transistor (with the effective gate area of ~0.0048 μm^2)[9] has only 48 defects. As such, it is no longer sufficient to consider just $<\Delta V_T>$; distribution of ΔV_T (designated as $P(\Delta V_T)$ for future reference) due to variation of interface defect generation must also be accounted for. Therefore, during product qualification one needs to estimate the statistics of defect generation up to transistor's lifetime, and ensure that the tails of $P(\Delta V_T)$ do not cross the reliability criteria during this period.

Among various BTI-induced ΔV_T phenomena, a PMOS-specific variant called NBTI has long been a major reliability concern in modern transistors[1, 10]. The generation of interface defect defines the dominant long-term component of NBTI relevant for circuit operation (which involves AC bias of variable frequency and duty cycle [11, 12]). It is generally assumed that interface defects arise from the dissociation of interfacial Si-H bonds at the silicon/dielectric interface; although involvements of other type of bonds have also been suggested[13]. The small dimension of modern transistors raises concerns in terms of N_{IT}-induced NBTI statistics. The importance of such

N_{IT}-induced ΔV_T distribution in circuit operation has already been extensively measured and characterized in many publications over the last few years [14-20]. Nevertheless, to this day, the *theoretical* $P(\Delta V_T)$ appropriate for NBTI degradation remains unspecified. For example, even though Poisson statistics was initially used (empirically) to interpret the spread of N_{IT}-induced ΔV_T [14], phenomenological statistical models like Gaussian or normal [9, 15, 16, 18], Skellam [17, 21], *etc.* have also been considered in subsequent years. Recently, negative ΔV_T tails are also observed in small transistors [17, 21], which has again been empirically explained by using the statistics of two *uncorrelated* Poisson-random process during N_{IT} generation [17], namely the dissociation of Si-H bond during the *creation process* and annealing of broken bonds during the *destruction process*. However, no systematic study has so far analyzed the *physical* origin of N_{IT} statistics in small transistors.

A theory of N_{IT}-induced $\Delta V_T@t_{STS}$ distribution should be based on two components: First, one must determine the temporal distribution of $N_{IT}@t_{STS}$ based on the dynamics of N_{IT} generation. This temporal distribution will then have to be convolved with the distribution of ΔV_T for a given number of N_{IT}, randomly distributed within the 2D silicon/dielectric interface [22-25]. In this paper, we first analyze the origin of temporal N_{IT} distribution (which is modeled within the framework of R-D theory) in section 2. We find that in small transistors the physical distribution of $t_{STS}@N_{IT}$ follows a log-normal distribution and the physical distribution of $N_{IT}@t_{STS}$ follows a skew normal distribution. However, at very long stress time or for large size transistors, both $N_{IT}@t_{STS}$ and $t_{STS}@N_{IT}$ statistics do revert back to the expected normal distribution. We also establish that the creation and destruction of N_{IT} is a correlated processes, hence ΔV_T due to N_{IT} formation should always be positive. Later, we study the effect of spatial distribution of finite number of N_{IT} in nanoscale transistors, in section 3, within a percolative problem represented by a random conductance network[26]. Therefore, we show that $P(\Delta V_T)$ for a particular number of interface defects is approximately exponential, with finite number of transistors having zero ΔV_T. In this case, our study is consistent with the one reported in Ref. 22-25. Finally, we combine the results of our temporal analysis (*i.e.*, skew-normal distribution for $N_{IT}@t_{STS}$) and spatial analysis (*i.e.*, exponential distribution for $\Delta V_T@N_{IT}$) to explain the reported $\Delta V_T@t_{STS}$ distribution of Ref. [19] in section 4.

2. Temporal N_{IT} Distribution: R-D Formalism

To understand the origin of N_{IT} statistics, we need a physical model to study the temporal evolution of N_{IT}. Among the available models for N_{IT} dynamics, Reaction-Diffusion (R-D) model have consistently interpreted a wide variety of NBTI experiments [4, 7, 12, 27-29] and variants of this model have been broadly adopted for process qualification [11, 30-32] and circuit design [32, 33]. Very briefly, the R-D model assumes dissociation (or reaction) of Si-H bond at the silicon/dielectric interface. The dissociation produces dangling Si- bonds (or interface defects) and atomic hydrogen H. Generated hydrogen species diffuse away from the interface in H and H_2 format. Indeed, it has been shown in Ref. [12, 27, 29] that N_{IT} dynamics (governed by R-D model with molecular hydrogen H_2 diffusion), along with hole trapping into pre-existing oxide defects, can explain many experimental features of NBTI (including stress-phase time exponent, ultra-fast relaxation, temperature dependence, field dependence, frequency dependence, duty cycle dependence) in transistors having nitrided and non-nitrided dielectric. For further details, please see extensive literature on the subject [12, 27, 29]. Although there have been other efforts to model NBTI [34, 35] based on a different formulation, these models are still evolving (*e.g.*, compare Ref. 34 to Ref. 35). In fact, it can be shown that regardless of the physical details, interpretation of NBTI phenomena like power-exponents, frequency-independence, duty-cycle dependence, *etc.* can be consistently explained using a physical model *only if* the physical model being used is mathematically equivalent to R-D model [36]. Therefore, in this paper we will focus on generalization and solution of statistical R-D model to interpret NBTI induced N_{IT} statistics.

Our analysis is relevant for transistors, where NBTI dynamics is dominated by interface defect components. In principle, depending on experimental conditions and on the type of dielectric under study, NBTI statistics can have contributions from both interface defects and hole trapping components[4, 7, 12, 30, 37]. Therefore, before comparing our theoretical predictions with measurements, one should first separate the N_{IT} components of NBTI (see Refs. [12, 29] for proposed methodology for separating N_{IT} component from NBTI measurement) and then apply our analysis to fit the N_{IT} statistics. Obviously, beyond the specific application to NBTI, the mathematical formulation of R-D statistics is completely general and is relevant for a wide variety of physical phenomenon including biosensors [38, 39], organic

solar cells [40], pattern formation[41], polymer phase segregation, *etc.*

2.1 R-D Model: Markov Chain Monte-Carlo Formalism

We obtain the statistics of $N_{IT}@t_{STS}$ by performing Markov Chain Monte-Carlo (MCMC) analysis of Reaction-Diffusion (R-D) model both by analytical and numerical calculations. In this regard, we use a first-order Markov process that involves a simple generalization of the Poisson process, typically used in NBTI literature[14, 17, 19, 21]. Breaking of Si-H bonds are statistically rare and memoryless. If there were *only* Si-H bond dissociation and diffusion of hydrogen species away from the interface (*i.e.*, there is a transition of particles from a given 'source' state to fully absorbing 'sink' state), then the process of Si-H bond dissociation can be well-described by a Poisson process. In practice, however, NBTI involves not only breaking of Si-H bonds and hydrogen diffusion away from the interface, but also back-diffusion of hydrogen species and repassivation of the dangling Si- bonds or interface states (*i.e.*, 'sink' sending back particles to the 'source'). Therefore, we consider interface defect generation to follow a first-order Markov process, where the occupancy at each state at each instant depends on the occupancy at neighboring states at previous instant. Indeed, such Markov process are regularly used to interpret other analogous Reaction-Diffusion problems, *e.g.*, capturing of particles in bio-sensors[39], chemical reactions at complex surfaces[42].

Therefore, we set up the Markov Chain transition matrix using R-D equations that governs the N_{IT} dynamics. Though R-D theory with H-H_2 diffusion is consistent with experimental data[4, 7, 12, 27-30], we develop the transition matrix both for H and H-H_2 diffusion. This is because the MCMC R-D analysis with H diffusion is analytically tractable and thus enables us to draw the key conclusions about a R-D system. Later, we also simulate $N_{IT}@t_{STS}$ statistics by considering (the experimentally-validated) H-H_2 as the diffusing species and show that the $N_{IT}@t_{STS}$ statistics with H-H_2 diffusion has similar signatures as the one with H diffusion.

2.1.1 Transition Matrix: H Diffusion

The rate equations governing the N_{IT} generation in R-D model, having atomic hydrogen (H) diffusion, have the following forms [2, 31]:

$$\frac{dN_{IT}}{dt} = k_F\left(N_0 - N_{IT}\right) - k_R N_{IT} N_H^{(0)}, \tag{1}$$

$$\frac{dN_H}{dt} = D_H \frac{d^2 N_H}{dx^2}, \tag{2}$$

$$\delta \frac{dN_H^{(0)}}{dt} = D_H \frac{dN_H^{(0)}}{dx} + \frac{dN_{IT}}{dt}. \tag{3}$$

Eqn. (1) represents passivation/de-passivation effects of Si-H bond, where k_F, k_R, N_0, N_{IT}, $N_H^{(0)}$ are defined as Si-H bond-breaking rate, Si-H bond-annealing rate, initial bond density available before stress, interface defect density and atomic hydrogen density at the Si/dielectric interface, respectively. Eqn. (2) describes diffusion (along x axis) of H, whereas Eqn. (3) corresponds to the conservation of fluxes of diffusing H near the interface (along x axis). In eqns. (2) and (3), D_H, N_H, and δ represent H diffusion coefficient, H concentration, and the interfacial thickness, respectively. *We reemphasize that although we use NBTI as a reference problem, the mathematical formulation discussed below is completely general and therefore would apply to biosensors, organic solar cells, and many other problems* [38-42].

To create the transition matrix for H-diffusion based R-D system, we first discretize eqns. (1)-(3) for constant time step Δt and constant grid size along the diffusion direction Δx [39, 43]. A rearrangement of the discretized version of R-D equations results –

$$\begin{aligned}\left[N_0 - N_{IT}\left(i+1\right)\right]/\Delta x \\ = \left(1-p_F\right)\left[N_0 - N_{IT}\left(i\right)\right]/\Delta x + p_R N_H^{(j=0)},\end{aligned} \tag{4}$$

$$\begin{aligned}N_H^{\,j}\left(i+1\right) = \left(1-2p_{D_H}\right)N_H^{\,j}\left(i\right) \\ + p_{D_H}\left[N_H^{\,j+1}\left(i\right) + N_H^{\,j-1}\left(i\right)\right],\end{aligned} \tag{5}$$

$$\begin{aligned}N_H^{\,j=0}\left(i+1\right) = p_F\left[N_0 - N_{IT}\left(i\right)\right]/\Delta x \\ + \left[1 - p_R - p_{D_H}\right]N_H^{(j=0)} + p_{D_H} N_H^{\,j=1}\left(i\right),\end{aligned} \tag{6}$$

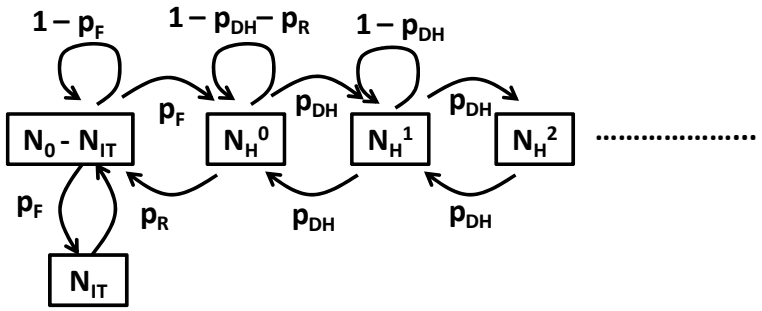

Figure 1: Markov model for probabilistic motion in an R-D system having H diffusion. The model is based on equations (4)-(6).

where $p_F = k_F\Delta t$, $p_R = k_R N_{IT}\Delta t/\Delta x$, and $p_{D_H} = D_H\Delta t\Delta x^{-2}$. Eqns. (4)-(6) enable us to define the Markov model of Figure 1, which is later used to analytically and numerically study the N_{IT} statistics using R-D theory. We can also express eqns. (4)-(6) in the following matrix form:

$$\begin{pmatrix} (N_0 - N_{IT})/\Delta x \\ N_H^{j=0} \\ N_H^{j=1} \\ N_H^{j=2} \\ \dots \\ \dots \end{pmatrix}_{i+1} = \begin{pmatrix} 1-p_F & p_R & 0 & \dots & 0 \\ p_F & 1-p_R-p_{D_H} & p_{D_H} & \dots & 0 \\ 0 & p_{D_H} & 1-p_{D_H} & \dots & 0 \\ 0 & 0 & p_{D_H} & \dots & 0 \\ & \dots & & \ddots & . \\ & \dots & & & . \end{pmatrix}_i \begin{pmatrix} (N_0 - N_{IT})/\Delta x \\ N_H^{j=0} \\ N_H^{j=1} \\ N_H^{j=2} \\ \dots \\ \dots \end{pmatrix}_i . \qquad (7)$$

$$\{\rho\}_{i+1} = [M]_i \{\rho\}_i$$

In eqn. (7), $[M]_i$ is the Markov model transition matrix defining the transition and staying probability of one particle after the i-th time step, $z_i = [(N_0\text{-}N_{IT})/\Delta x\ N_H^{j=0}\ N_H^{j=1}\ \dots]^T$ is a vector for storing the interface defect density and hydrogen concentration at different spatial grid points j. The diagonal elements of $[M]_i$ indicate the 'staying' probability of each Monte-Carlo particle; whereas the off-diagonal elements indicate the 'transition' probabilities in forward or reverse direction within the simulation domain. It is to be noted here that Eqn. (7) is similar to the one developed in Ref. 39, except $[M]_i$ was assumed to be time-invariant in Ref. 39. However, this is not the case in the R-D system under study, because for N_{IT} generation p_R is time-dependent.

We use eqn. (7) to determine the mean value of N_{IT} and $N_H{}^j$ at different $t_{STS} = [t_1\ t_2\ t_3\ \dots]$. To do this, we define $\rho(t_{STS} = 0) = \{\rho\}_0 = [N_0/\Delta x\ 0\ 0\ \dots]^T$ and hence, obtain $\{\rho\}_i$ at different t_i using $\{\rho\}_i = [M]_{i-1}\ \{\rho\}_{i-1}$. Next, we determine the statistics of $\{\rho\}_i$ through Monte-Carlo simulation. During Monte-Carlo simulation, we use $\{\rho\}_0 = [N_0LW\ 0\ 0\ \dots]^T$ and the transition, staying probabilities of eqn. (7) at each time step t_i to determine the statistics of R-D system.

2.1.2 Transition Matrix: H-H_2 Diffusion

The diffusion equations governing the N_{IT} generation (along with eqn. (1)) in R-D model, having both H and H_2 diffusion, have the following form [4, 44]:

$$\delta\frac{dN_H^{(0)}}{dt} = D_H\frac{dN_H^{(0)}}{dz} + \frac{dN_{IT}}{dt} - \delta k_H\left[N_H^{(0)}\right]^2 + \delta k_{H2}N_{H2}^{(0)},$$
$$\delta\frac{dN_{H2}^{(0)}}{dt} = D_{H2}\frac{dN_{H2}^{(0)}}{dz} + \frac{\delta}{2}k_H\left[N_H^{(0)}\right]^2 - \frac{\delta}{2}k_{H2}N_{H2}^{(0)}, \qquad (8)$$

$$\frac{dN_H}{dt} = D_H\frac{d^2N_H}{dz^2} - k_H{N_H}^2 + k_{H2}N_{H2},$$
$$\frac{dN_{H2}}{dt} = D_{H2}\frac{d^2N_{H2}}{dz^2} + \frac{1}{2}k_H{N_H}^2 - \frac{1}{2}k_{H2}N_{H2}. \qquad (9)$$

Here, eqn. (8) corresponds to the conservation of fluxes of diffusing hydrogen species (H and H_2) near the interface

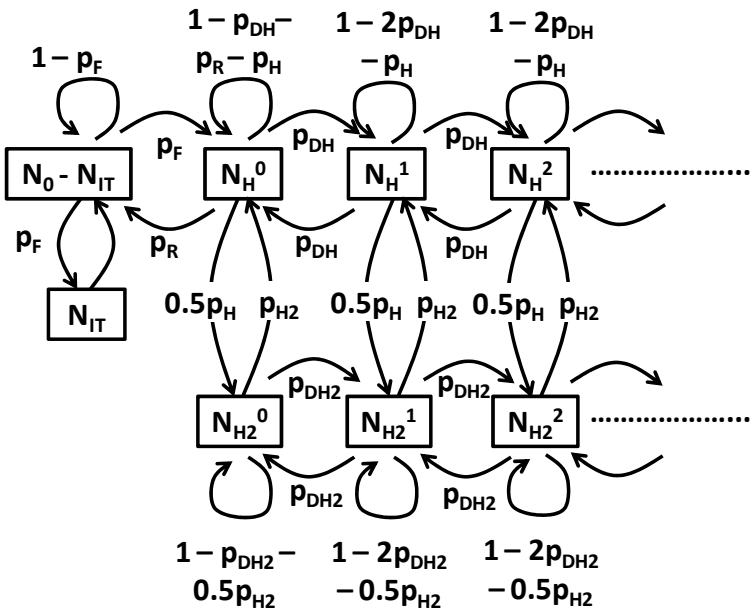

Figure 2: Markov model for probabilistic motion in an R-D system having H-H_2 diffusion. The model is based on eqns. (1),(8)-(9).

(along x axis), whereas eqn. (9) describes diffusion (along x axis) of H and H_2. The $k_H N_H^{\,2}$ and $k_{H2} N_{H2}$ terms in eqn. (8) incorporate the H-H_2 conversion within the generalized R-D framework. Among the symbols used in eqns. (8) and (9), k_H, k_{H2} represent generation and dissociation rates of H_2; D_H, D_{H2} represent diffusion coefficients for H and H_2; and N_H, N_{H2} represent the concentration of atomic and molecular hydrogen.

Now to study the N_{IT} statistics for H-H_2 R-D model, we again discretize eqns. (1),(8)-(9). A rearrangement of the discretized version of R-D equations enables us to define the Markov model of Figure 2 and transition matrix in eqn. (10), where $p_{D_{H_2}} = D_{H2}\Delta t \Delta x^{-2}$, $p_{H,j} = k_H N_H^{\,j} \Delta t$, and $p_{H_2,j} = k_{H2}\Delta t$.

$$\left[\left(N_0 - N_{IT}\right)/\Delta x \;\; N_H^{j=0} \;\; N_H^{j=1} \;\; N_H^{j=2} \;\ldots\ldots\; N_{H_2}^{j=0} \;\; N_{H_2}^{j=1} \;\; N_{H_2}^{j=2} \;\ldots\ldots\right]_{i+1}^{T} =$$

$$\begin{pmatrix}
1-p_F & p_R & 0 & 0 & 0 & 0 & 0 & 0 \\
p_F & 1-p_r-p_{D_H}-p_{H,0} & p_{D_H} & 0 & p_{H_2,0} & 0 & 0 & 0 \\
0 & p_{D_H} & 1-2p_{D_H}-p_{H,1} & 0 & 0 & p_{H_2,1} & 0 & 0 \\
0 & 0 & p_{D_H} & 0 & 0 & 0 & p_{H_2,2} & 0 \\
\ldots & \ldots & \ddots & \ldots & \ldots & \ldots & \ddots & \ldots \\
\ldots & \ldots & & \ldots & \ldots & \ldots & & \ldots \\
0 & 0.5p_{H,0} & 0 & 0 & 1-p_{D_{H_2}}-0.5p_{H_2,0} & p_{D_{H_2}} & 0 & 0 \\
0 & 0 & 0.5p_{H,1} & 0 & p_{D_{H_2}} & 1-2p_{D_{H_2}}-0.5p_{H_2,1} & p_{D_{H_2}} & 0 \\
0 & 0 & 0 & 0 & 0 & p_{D_{H_2}} & 1-2p_{D_{H_2}}-0.5p_{H_2,2} & 0 \\
\ldots & \ldots & \ddots & \ldots & \ldots & \ldots & \ddots & \ldots \\
\ldots & \ldots & & \ldots & \ldots & \ldots & & \ldots
\end{pmatrix} \tag{10}$$

$$\left[\left(N_0 - N_{IT}\right)/\Delta x \;\; N_H^{j=0} \;\; N_H^{j=1} \;\; N_H^{j=2} \;\ldots\ldots\; N_{H_2}^{j=0} \;\; N_{H_2}^{j=1} \;\; N_{H_2}^{j=2} \;\ldots\ldots\right]_{i}^{T}.$$

$$or, \quad \{\rho\}_{i+1} = [M]_i \{\rho\}_i$$

The definition of matrix elements in eqn. (10) are similar to the one in eqn. (7), except eqn. (10) has some extra terms related to H_2 diffusion and H-H_2 inter-conversion. Also, the steps for performing Monte-Carlo simulation are similar to the one stated at the end of section 2.1.1.

2.2 Statistics of R-D System

In this section, we use the transition matrix, defined in section 2.1, to obtain the statistics of N_{IT}. First, we analytically and numerically study the N_{IT} statistics by considering H as the diffusing species. Later, we numerically study the N_{IT} statistics by considering both H and H_2 as the diffusing species and show that the resultant N_{IT} statistics has similar signatures as the one with H diffusion.

2.2.1 N_{IT} Statistics for H Diffusion: Analytical Calculation

Before performing MCMC simulation numerically, let us consider the statistics of H-diffusion based R-D system through an analytical calculation of the moments of the distribution. This calculation enables us to interpret the simulation results, to be discussed later in section 2.2.2.

Statistics for t_{STS}@N_{IT}

Power series generating functions[45] are well adapted to calculate the moments of t_{STS}@N_{IT} distribution by using the transition and staying probabilities of the Markov transition matrix of eqn. (7). It can be shown using generating function that the mean t_{STS} for a particular level of N_{IT} is [46-48]:

$$\mu_{0,S} = \left[\sum_{k=0}^{S-1}\frac{1}{p_k} + \sum_{k=0}^{S-2}\frac{1}{p_k}\sum_{i=k+1}^{S-1}\prod_{j=k+1}^{i}\frac{q_j}{p_j}\right]\Delta t, \qquad (11)$$

where p's and q's are the right (moving away from the Si/dielectric interface in the R-D system under study) and left (moving towards the Si/dielectric interface) transition probabilities, respectively; S is the average number of Monte-Carlo (or random walk) steps taken for the generated N_{IT}; for example, $S = 0$ means no Si-H bond dissociation, $S = 1$ means Si-H bond dissociation with insignificant diffusion, and $S > 1$ means that the dissociated H has diffused (on average) a distance $(S\text{-}1)\Delta x$ away from the interface. For eqn. (7), $p_0 = p_F = k_F\Delta t$, $q_1 = p_R = k_R N_{IT}\Delta t/\Delta x$, and $p_1 = p_2 = p_3 = \ldots\ldots = p_{S-1} = q_2 = q_3 = \ldots\ldots = q_S = p_{D_H} = D_H\Delta t\Delta x^{-2}$. Hence, using eqn. (11), we calculate –

$$\mu_{0,S} = \left[\frac{1}{k_F\Delta t} + \frac{S-1}{D_H\Delta t\Delta x^{-2}}\left(\frac{S}{2} + \frac{k_R N_{IT}/\Delta x}{k_F}\right)\right]\Delta t. \qquad (12)$$

Similarly, using generating function[45], we can also calculate variance of t_{STS}@N_{IT} distribution:

$$\sigma^2_{0,S} = \left[\begin{array}{l} \dfrac{1}{\left(k_F\Delta t\right)^2} - \dfrac{1}{k_F\Delta t} + \dfrac{S\left(S+1\right)\left(S^2+S+1\right)}{6\left(D_H\Delta t\Delta x^{-2}\right)^2} + \dfrac{S}{D_H\Delta t\Delta x^{-2}} \\ \left(\dfrac{2k_R N_{IT}/\Delta x}{\left(k_F\Delta t\right)^2} - \dfrac{2k_R N_{IT}/\Delta x}{k_F\Delta t} - \dfrac{S+1}{2}\right) \\ + \dfrac{S\left(S+1\right)\left(2S+1\right)}{3\left(D_H\Delta t\Delta x^{-2}\right)^2}\dfrac{k_R N_{IT}/\Delta x}{k_F\Delta t} + + \dfrac{S^2}{\left(D_H\Delta t\Delta x^{-2}\right)^2}\left(\dfrac{k_R N_{IT}/\Delta x}{k_F\Delta t}\right)^2 \end{array}\right]\left(\Delta t\right)^2. \qquad (13)$$

Now, in the reaction (when, $S \sim 0$) and diffusion (when, $S >> 1$) limits of the H-diffusion based R-D system, eqns. (12)-(13) reduces to –

$$\mu_{0,S} \simeq \frac{1}{k_F}; \qquad \sigma^2_{0,S} \simeq \frac{1}{{k_F}^2}, \qquad \text{(Reaction regime)} \qquad (14)$$

$$\mu_{0,S} \simeq \frac{S^2}{2D_H\Delta x^{-2}}; \qquad \sigma^2_{0,S} \simeq \frac{S^4}{6\left(D_H\Delta x^{-2}\right)^2}. \qquad \text{(Diffusion regime)} \qquad (15)$$

Here, eqn. (14) reflects that if there were no diffusion or annealing (*i.e.*, both D_H and k_R are negligible), Si-H bond dissociation will occur after a mean time of $\sim 1/k_F$, having a standard deviation of the same order. Interestingly, eqns. (14) and (15) suggest that both in the reaction and diffusion limits of the R-D system, $\mu_{0,S} \sim \sigma_{0,S}$, which is a general characteristic for a log-normal distribution, with $\sqrt{\exp\sigma^2 - 1} \sim 1$ in the following expression for the probability distribution function (PDF):

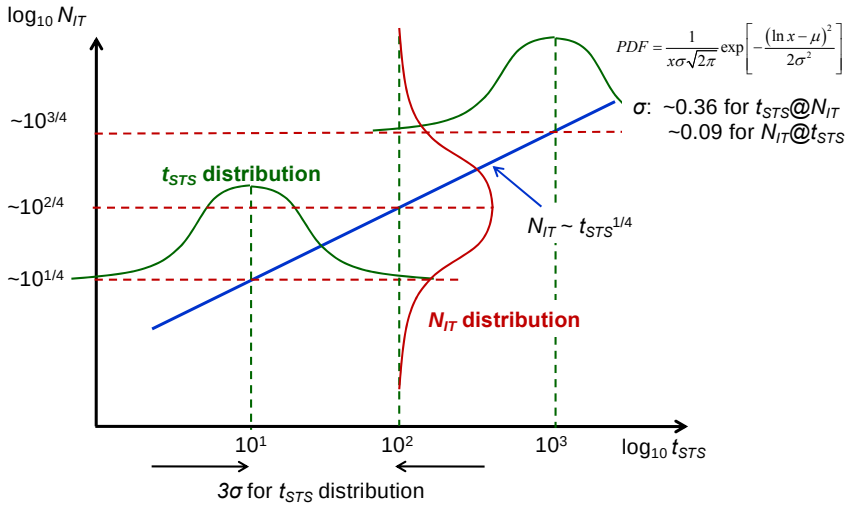

Figure 3: A schematic to illustrate the idea that a log-normal distribution for $t_{STS}@N_{IT}$ guarantees a log-normal distribution for $N_{IT}@t_{STS}$ with constant σ for the distribution expressed in the form of eqn. (16).

$$PDF = \frac{1}{x\sigma\sqrt{2\pi}} \exp\left[-\frac{(\ln x - \mu)^2}{2\sigma^2}\right] \qquad (16)$$

For the $t_{STS}@N_{IT}$ distribution, we calculate $\mu = \ln \mu_{0,S} - 0.5 \ln\left(1 + \sigma_{0,S}^2 / \mu_{0,S}^2\right) \sim \ln \mu_{0,S}$ and $\sigma = \sqrt{\ln\left(1 + \sigma_{0,S}^2 / \mu_{0,S}^2\right)} \sim \sqrt{\ln 2}$ (or 0.362 in the base-10 log-scale). Thus $\sqrt{\exp \sigma^2 - 1} \sim 1.16$ for our case, such that, $\mu_{0,S} \sim \sigma_{0,S} \sim \exp\left(\mu + \sigma^2/2\right)$. Therefore, the generating function calculation anticipates a log-normal distribution for $t_{STS}@N_{IT}$, at any t_{STS}, with an approximately constant σ. Obviously, for large t_{STS} or for large-area transistors, where $\mu_{0,S}$ is very large, log-normal distribution of eqn. (16) reverts back to the well-known Gaussian or normal distribution.

Statistics for $N_{IT}@t_{STS}$

So far, we have developed an analytical formalism for predicting the distribution of $t_{STS}@N_{IT}$ in the last few paragraphs. We must now invert this distribution graphically into $N_{IT}@t_{STS}$ distribution to compare the predicted results with those measured from NBTI experiments. R-D system with H-diffusion has a power-law time exponent $n \sim 1$ in the reaction regime and $n \sim 1/4$ in the diffusion regime. Such power-law behavior suggests that (see Figure 3) *when the $t_{STS}@N_{IT}$ distribution is log-normal (following eqn. (16)) with constant σ, the $N_{IT}@t_{STS}$ distribution should also be log-normal with constant σ.* Now, the σ for the $N_{IT}@t_{STS}$ distribution will be n times the σ for the $t_{STS}@N_{IT}$ distribution (as graphically illustrated in Figure 3). Thus, the $N_{IT}@t_{STS}$ distribution will have a constant σ ~0.362 (in base-10 log-scale) in reaction regime and σ~0.0905 in the H-diffusion regime. Our MCMC simulation also suggests that one can readily observe a log-normal distribution for $t_{STS}@N_{IT}$ (see Figure 6). However, the constraints of $N_{IT} > 0$ and presence of small σ (in the diffusion regime) results in a skew-normal or normal distribution for $N_{IT}@t_{STS}$ (see Figure 6 and Figure 8), as discussed later.

2.2.2 N_{IT} Statistics for H Diffusion: MCMC Simulation Results

Before studying the statistics of $N_{IT}@t_{STS}$, we first confirm that our MCMC result is consistent with the continuum simulation (obtained by numerically solving eqns. (1)-(3)). As shown in Figure 4, the *average* of about 1000 MCMC simulations has remarkable consistency with the continuum simulation for a large (L = 100nm; W = 1um) transistor (Figure 4a), as well as for a small (L = 50nm; W = 100nm) transistor (Figure 4b). However, average N_{IT} is not the only quantity of interest in small transistors; we need to know the statistics. In the subsequent sections, we simulate the statistics of N_{IT} generation using eqn. (7) and show that our MCMC simulation results are consistent with the analytical calculations of section 2.2.1.

As shown in Figure 6, the distribution of $t_{STS}@N_{IT}$ is symmetric around the median value in a semilog-x plot, while only being cut-off at the two ends by the sampling time and the simulation length. As such, it is evident that the $t_{STS}@N_{IT}$ distribution follows a log-normal behavior (as predicted from our analytical calculation in section 2.2.1),

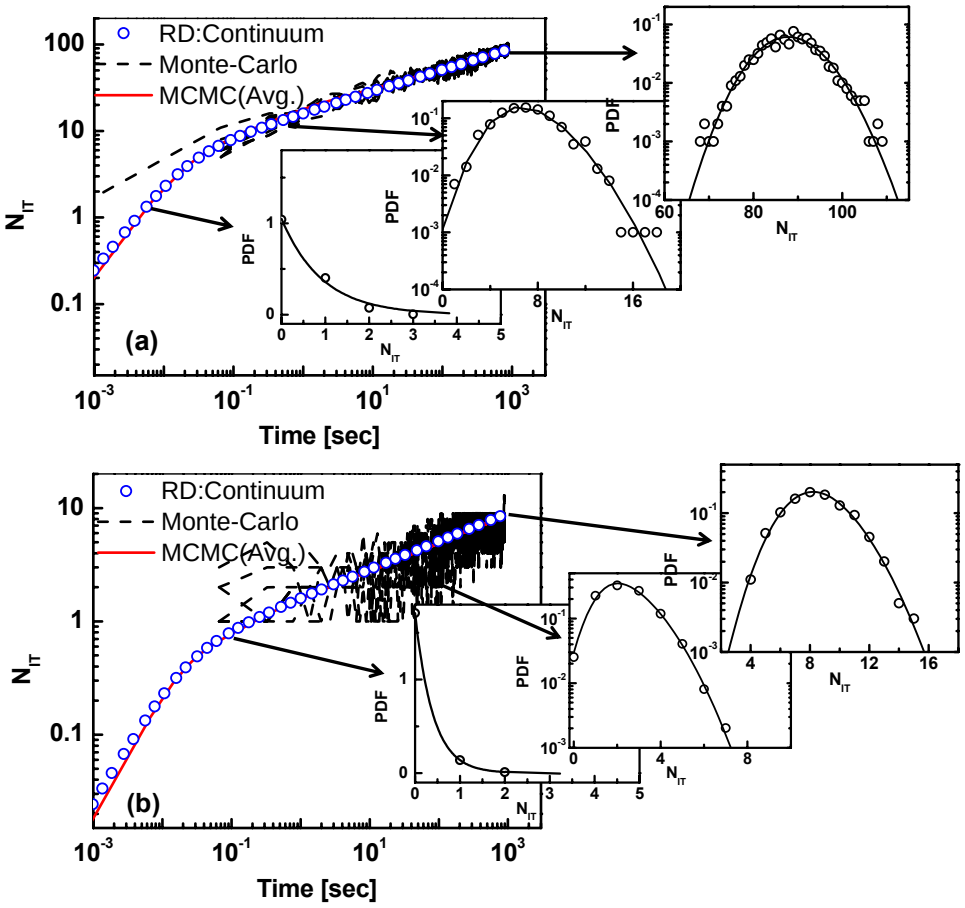

Figure 4: Time dependence and PDF of interface defect generation for (a) large transistor (L = 100nm, W = 1um) and (b) small transistor (L = 50nm, W = 100nm) using $N_0 = 5\text{x}10^{12}$ cm^{-2}, $k_F = 0.1$ sec^{-1}, $k_R = 2\text{x}10^{-16}$ cm^{-3}sec^{-1}, and $D_H = 10^{-13}$ cm^2-sec^{-1}. For the large transistor, the PDF evolves from skewed normal (in the reaction phase) to a normal (in the diffusion phase) distribution. However, for the small transistor, the distribution stays skewed normal, even in the diffusion phase, which is commonly captured within the measurement window of NBTI measurement scheme.

having its median point being tracked by the continuum simulation. More interestingly, the log-normal distributions of Figure 6 has a constant $\sigma \sim 0.5$ (at all t_{STS}), which is a little larger than the one obtained from our approximate analysis in section 2.2.1.

Now, given that the $t_{STS}@N_{IT}$ distribution is log-normal, let us study the distribution of $N_{IT}@t_{STS}$ (commonly measured in NBTI experiments) for the *large transistor* (L = 100nm, W = 1um). Though the distribution is clearly Gaussian at longer simulation time, it shows significant skewness at shorter time (insets of Figure 4a). However, such skewness is only observed at a mean N_{IT}, $\mu_{IT} << 10^{10}$ cm^{-2} (or $\Delta V_{T,mean} < 1$mV for a transistor with $EOT \sim 1$nm), which is seldom reported in conventional NBTI statistics measurement. *On the other hand, for small transistor (L = 50nm, W = 100 nm), $N_{IT}@t_{STS}$ distribution do not become Gaussian, even for a $\mu_{IT} \sim 2\text{x}10^{11}$ cm^{-2} (insets of* Figure 4*b), commonly measured in NBTI experiments.* The standard deviation of the N_{IT} distribution (σ_{IT}) always increases with mean μ_{IT} (see Figure 5a) and the distribution has significant positive skewness, γ_{IT} (see Figure 5). Note that such increase of distribution spread with mean and existence of a skewed distribution are regularly reported in NBTI experiments [9, 14, 16, 17, 19, 21]. Based on the above analysis, the following expression of skewed Gaussian distribution [49] is used to fit the $N_{IT}@t_{STS}$ distribution in small-size transistors:

$$P(N_{IT}) = 2\phi\left(\frac{N_{IT}-\xi_{IT}}{\omega_{IT}}\right)\Phi\left(\alpha_{IT}\frac{N_{IT}-\xi_{IT}}{\omega_{IT}}\right), \quad (17)$$

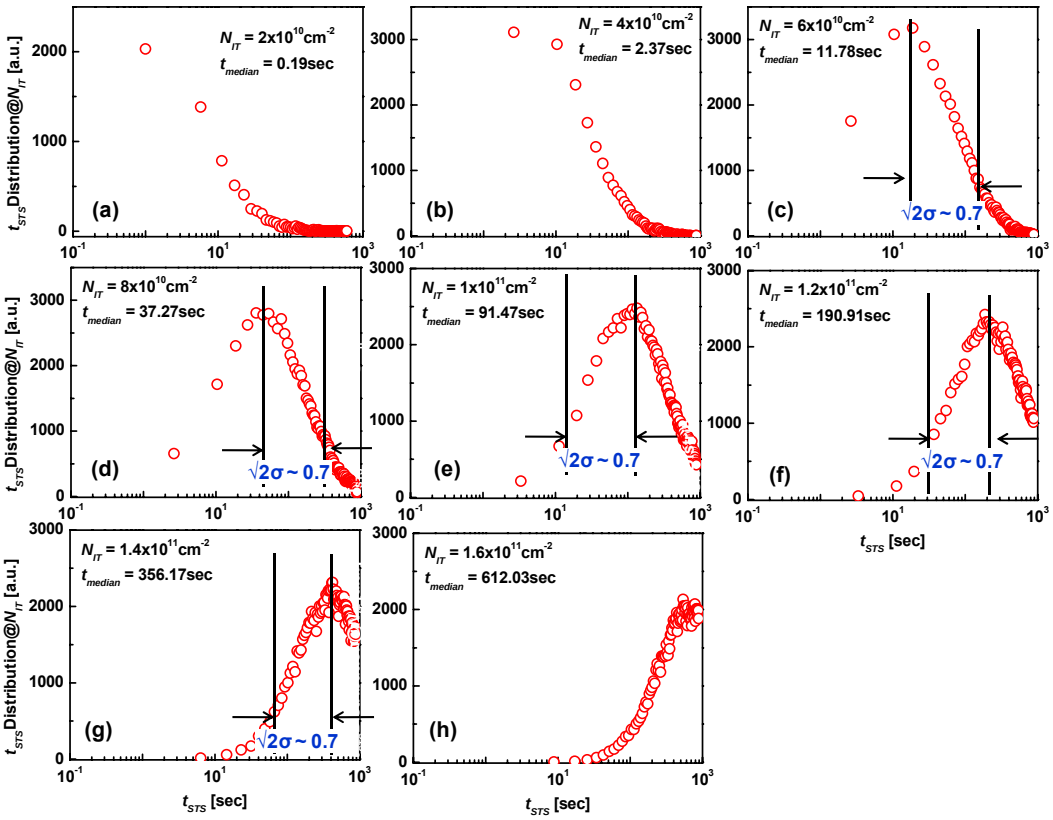

Figure 6: Distribution of t_{STS} at different levels of N_{IT} obtained from 1000 MCMC simulation in the small transistor under study. The distribution is clearly log-normal, having cut-off at t_{STS} ~ 0.1 sec (sampling time) and t_{STS} ~ 10^3 sec (maximum length of MCMC simulation). The distribution also has constant standard deviation in the semilog-x plot, as expected from the analytical calculation.

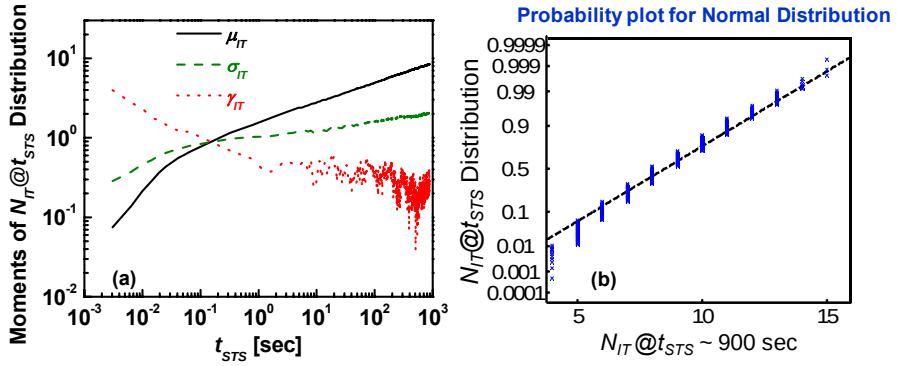

Figure 5: (a) Though the mean (μ_{IT}) and standard deviation (σ_{IT}) increases with t_{STS} with a power-law time exponent (~0.25 for μ_{IT} and ~0.1 for σ_{IT}), skewness (γ_{IT}) reduces with t_{STS}. Such reduction in γ_{IT} indicates that the distribution is approaching towards a Gaussian one at longer t_{STS}. (b) The normal probability plot also confirms the existence of skewness at t_{STS} ~ 900sec for Figure 4b.

where $\varphi(x)$ and $\Phi(x)$ indicate the probability distribution function (PDF) and cumulative distribution function (CDF) of a Gaussian distribution, and ξ_{IT}, ω_{IT}, α_{IT} have the following relationship with the μ_{IT}, σ_{IT}, and γ_{IT} of the N_{IT}@t_{STS} distribution[49]:

$$\mu_{IT} = \xi_{IT} + \omega_{IT}\delta_{IT}\sqrt{2/\pi},$$
$$\sigma_{IT} = \omega_{IT}\sqrt{1-2\delta_{IT}^{\,2}/\pi},$$
$$\delta_{IT} = \alpha_{IT}\Big/\sqrt{1+\alpha_{IT}^{\,2}},$$
$$\gamma_{IT} = \frac{4-\pi}{2}\frac{\left(\delta_{IT}\sqrt{2/\pi}\right)^3}{\left(1-2\delta_{IT}^{\,2}/\pi\right)^{3/2}}. \qquad (18)$$

Now for fitting the $N_{IT}@t_{STS}$ statistics using eqn. (17), we first need to estimate μ_{IT}, σ_{IT}, and γ_{IT} of the $N_{IT}@t_{STS}$ distribution. Then, we estimate the skew-normal distribution parameters ξ_{IT}, ω_{IT}, and α_{IT} using eqn. (18) and hence check the goodness of eqn. (17) in matching the $N_{IT}@t_{STS}$ distribution. Figure 8 shows the $N_{IT}@t_{STS}$ distribution, obtained from 10000 MCMC simulations, in the small transistor (L = 50nm; W = 100nm) under study at

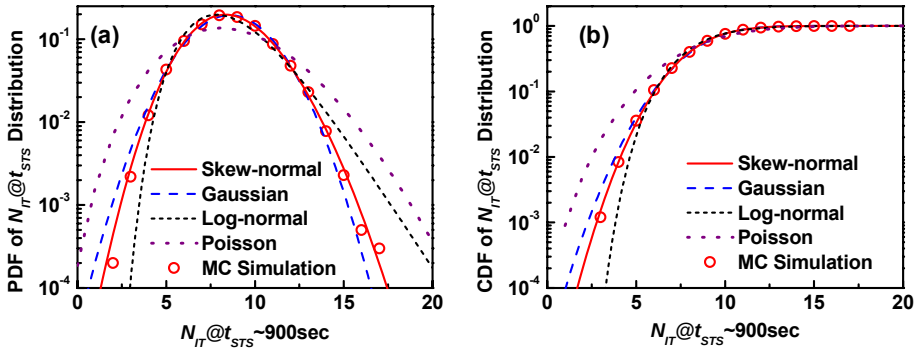

Figure 8: Both PDF and CDF of $N_{IT}@t_{STS}$ ~ 900sec can consistently be explained using the skewed normal distribution of eqns. (17)-(18). Other statistics (Gaussian, Poisson, and log-normal) are also fitted with the simulated data using maximum likelihood estimation (MLE). SSE for different distribution functions are: $4.6\text{x}10^{-5}$ for skew-normal, $4\text{x}10^{-4}$ for Gaussian, $11.4\text{x}10^{-3}$ for Poisson, and $2\text{x}10^{-3}$ for log-normal.

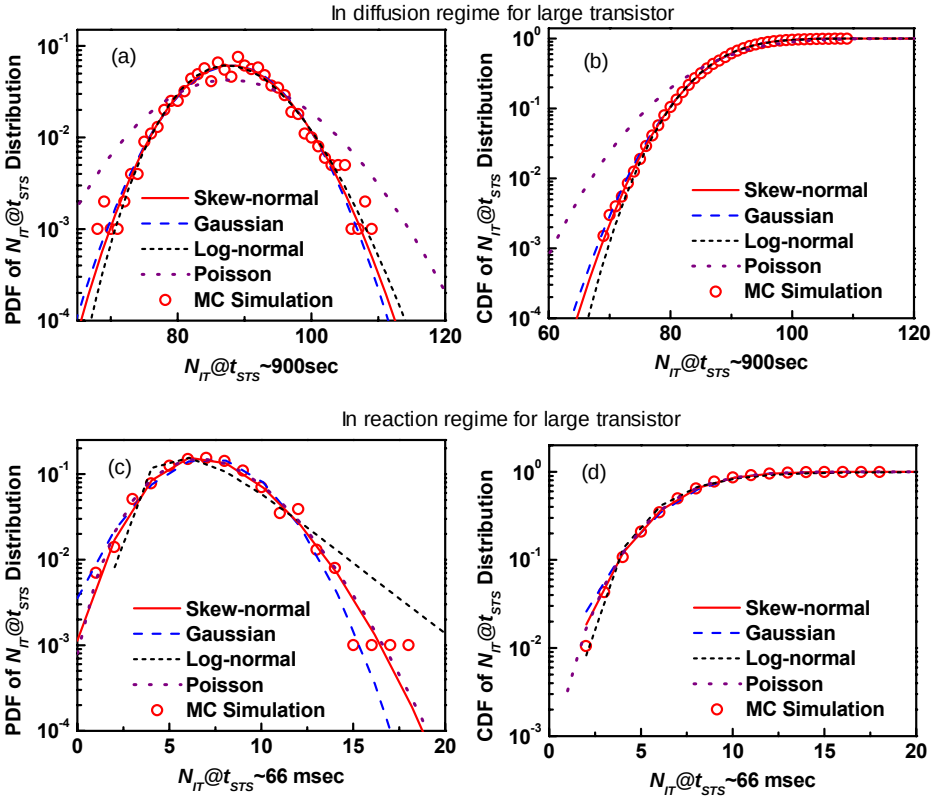

Figure 7: (a,b) PDF and CDF for a large transistor in the diffusion regime showing no distinction between a log-normal and normal distribution. (c,d) Log-normal was expected for the same transistor in the reaction regime; however, in this reaction regime, the distribution gets constraint by $N_{IT} > 0$ and gets skewed towards positive side of N_{IT} as in Figure 8.

μ_{IT} ~10^{11} cm^{-2} and skew-normal distribution (eqns. (17)-(18)) indeed shows the best match compared to other distribution functions. Sum of squares due to error for skew-normal distribution is ~4.6x10^{-5}, which is at least an order of magnitude smaller than the same obtained for other distribution functions.

2.2.3 N_{IT} Statistics for H Diffusion: Analytical vs Numerical Results

Let us now compare the N_{IT} statistics obtained from our analytical and numerical analysis. Figure 3 suggests that both $N_{IT}@t_{STS}$ and $t_{STS}@N_{IT}$ statistics should follow log-normal distribution, whereas, our MCMC simulation suggests a log-normal behavior only for the $t_{STS}@N_{IT}$ distribution (Figure 6), but not for the $N_{IT}@t_{STS}$ distribution (see insets of Figure 4 and Figure 8). This is because σ of eqn. (16) for the $N_{IT}@t_{STS}$ distribution is much smaller than μ, which is not the case for the $t_{STS}@N_{IT}$ distribution. As explained in Figure 3, for the H diffusion regime with time exponent, $n \sim 1/4$, σ for $N_{IT}@t_{STS}$ in the diffusion regime is 4 times smaller than the σ for $t_{STS}@N_{IT}$. As a result of this small σ in the diffusion regime for the $N_{IT}@t_{STS}$ distribution, the log-normal distribution for the $N_{IT}@t_{STS}$ statistics approaches a normal distribution. As such, both the log-normal and normal fitting in Figure 7a for the large transistor suggests indistinguishable behavior. Finally, the constraint of $N_{IT} > 0$ requires that the $N_{IT}@t_{STS}$ statistics at small μ_{IT} (as is the case in small transistors) is described by a skew-normal, rather than a normal distribution.

Note that, it is also possible to observe log-normal $N_{IT}@t_{STS}$ distribution in the reaction-regime for the large transistor, where σ for the $N_{IT}@t_{STS}$ distribution is comparatively larger than σ in the diffusion regime. However, in such case the $N_{IT}@t_{STS}$ distribution is skewed towards the positive side (see Figure 7b) due to the constraint of $N_{IT} > 0$. Therefore, though log-normal

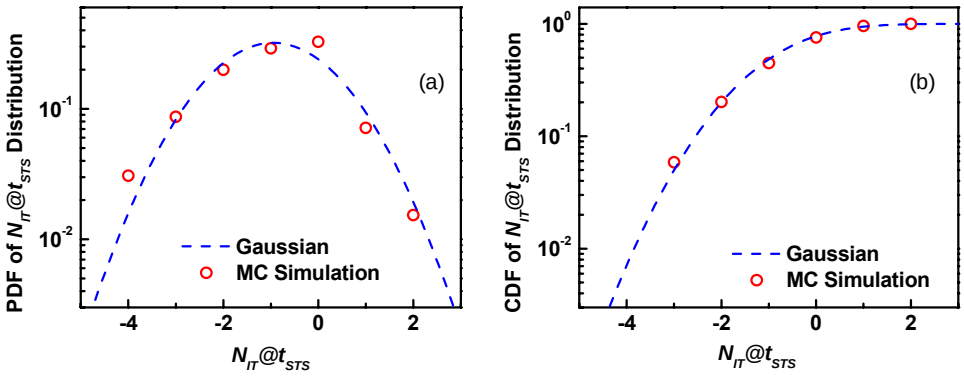

Figure 9: (a) PDF and (b) CDF of N_{IT}-induced ΔV_T for a small transistor having pre-existing interface defect. The distribution can explain the observation of negative ΔV_T tails in the experiments of Ref. 21.

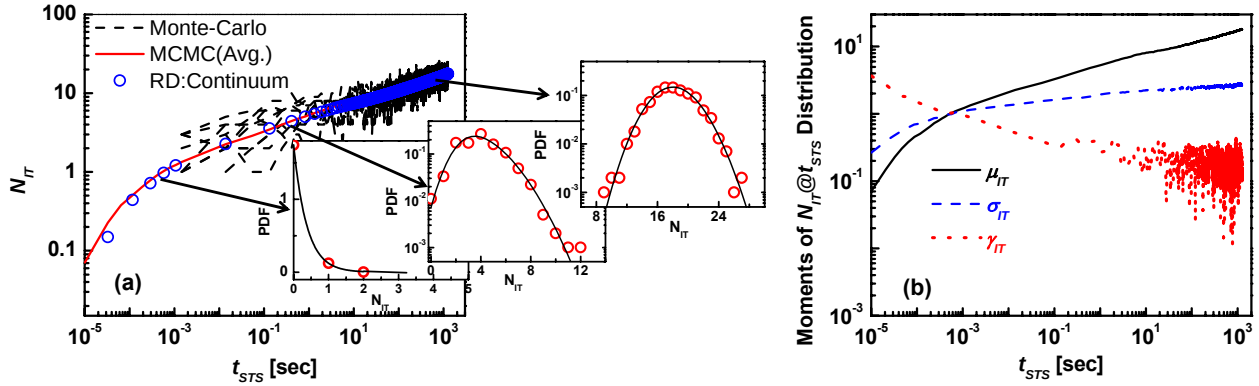

Figure 10: (a) Time dependence and PDF of interface defect generation for a small transistor (L = 50nm, W = 100nm) using N_0 = 5x10^{12} cm^{-2}, k_F = 30 sec^{-1}, k_R = 2x10^{-15} cm^{-3}sec^{-1}, $D_H = D_{H2}$ = 10^{-13} cm^2-sec^{-1}, k_H = 9x10^{-15} cm^{-3}sec^{-1}, and k_{H2} = 600 sec^{-1}. Similar to the observation in Figure 4b, the distribution stays skew normal, unless the magnitude of mean N_{IT} (μ_{IT}) is quite large. (b) Both mean and standard deviation increases with t_{STS} with a power-law time exponent (~0.17 for μ_{IT} and ~0.04 for σ_{IT}), however, positive skewness γ_{IT} reduced with t_{STS}.

distribution is physically expected for the $N_{IT}@t_{STS}$ statistics, due to the – (a) constraint of small σ for eqn. (16) the $N_{IT}@t_{STS}$ statistics approaches a normal distribution at comparatively larger μ_{IT}, (b) constraint of $N_{IT} > 0$, the $N_{IT}@t_{STS}$ statistics approaches a skew-normal distribution for smaller μ_{IT}.

2.2.4 Correlated N_{IT} Creation and Destruction

As evident from our discussions so far, the statistics of a R-D system follows a log-normal distribution of eqn. (16), unless it is modified to a normal distribution for small σ, or is modified to a skew-normal distribution due to the $N_{IT} > 0$ constraints. Let us now discuss the correlation between the creation (Si-H bond dissociation) and destruction (Si- bond annealing) processes of N_{IT} generation. Such correlation provides a natural physical interpretation for the recently observed negative ΔV_T tails in NBTI experiments [17, 21].

In all our MCMC R-D simulations, the creation and destruction of N_{IT}, as well as diffusion of H, are considered as separate random processes. However, destruction of N_{IT}, through the second term in right-hand side of eqn. (1), is only possible for $N_{IT} > 0$. This dictates that the creation and destruction processes in R-D model can not be uncorrelated and consequently generated N_{IT} (hence ΔV_T) can not be negative. In support of this argument, none of our MCMC R-D simulation show negative N_{IT}-induced ΔV_T, suggesting a correlation between the creation and destruction processes in the R-D system. Thus, the observation of negative ΔV_T tails in Ref. [17, 21] may be a consequence of N_{IT} relaxation in transistors having pre-existing N_{IT} or higher initial threshold voltage V_{T0}. In these higher V_T transistors, the pre-existing N_{IT} gets annealed during the NBTI stress, and therefore can result in a negative ΔV_T (see Figure 9).

2.2.5 N_{IT} Statistics for H-H_2 Diffusion: MCMC Simulation

In the sections 2.2.1-2.2.4, we have analyzed the statistical properties of R-D system with atomic hydrogen H as the diffusing species. Here, we repeat the same mathematical formulation for the R-D system having both atomic and molecular hydrogen (H and H_2) as the diffusing species. Such H-H_2 R-D system results in a power-law time exponent, $n \sim 1/6$, and hence is more relevant for N_{IT} generation under NBTI stress. As we did for the H-based R-D system, we use the transition matrix of eqn. (10) to simulate the statistics of N_{IT}.

After setting the simulation framework, we check the

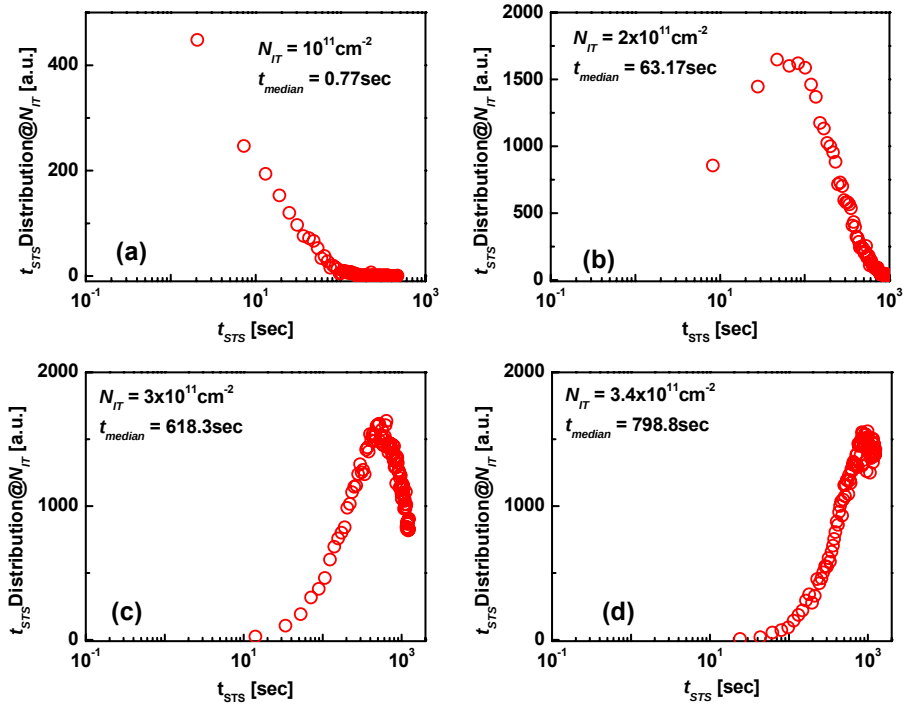

Figure 11: Distribution of t_{STS} at different levels of N_{IT} obtained from 1000 MCMC simulation (for R-D system with H-H_2 diffusion) in the small transistor under study. The distribution is clearly log-normal, having cut-off at $t_{STS} \sim 0.1$sec (sampling time) and $t_{STS} \sim 10^3$sec (maximum length of MCMC simulation).

consistency of our MCMC simulation (obtained using eqn. (10)) with the continuum simulation (obtained by numerically solving eqns. (1),(8)-(9)). As shown in Figure 10a, the average of about 1000 MCMC simulations has remarkable consistency with the continuum simulation results for a small (L = 50nm; W = 100nm) transistor. Next, we study the distribution of N_{IT} for the *small transistor* at different time steps. Again, similar to the H-based R-D system, N_{IT} distribution reaches a normal distribution only for higher density of N_{IT} (insets of Figure 10a). Moreover, an analysis of the moments of the $N_{IT}@t_{STS}$ distribution shows an increase in the standard deviation of the distribution (σ_{IT}) with the increase in mean (μ_{IT}) (see Figure 10b). The distribution also has positive skewness at lower μ_{IT} (see Figure 10b), which reduces with increase in μ_{IT}.

Now, let us review the $t_{STS}@N_{IT}$ statistics for the H-H_2 R-D system. Similar to the case for H diffusion based R-D system (Figure 6), H-H_2 R-D system follows a log-normal distribution (Figure 11) and is curtailed at the two ends by the sampling time and the integrated simulation time. Thus, we conclude that R-D system with H-H_2 diffusion has similar statistical nature as the R-D system with H diffusion.

3. ΔV_T Statistics: Spatial Distribution of N_{IT}

The $N_{IT}@t_{STS}$ statistics, presented in section 2, considers the time-dependent statistical properties of Si-H bond dissociation and resultant hydrogen diffusion as a 1D problem; *i.e.*, we have a point source of hydrogen at the interface and the hydrogen is diffusing vertically through the gate and poly-silicon. This temporal aspect of statistical solution of the R-D system is completely general and is application to any R-D system. However, for MOSFET, Si-H bonds (and generated N_{IT}) are distributed along the 2D surface at the silicon/dielectric interface. So, for a particular amount of N_{IT}, there is an additional issue with the *spatial* distribution of N_{IT} over the entire transistor structure, which can give rise to different ΔV_T for same number of N_{IT} [22-25].

Such distribution of ΔV_T for same N_{IT} (at a given time) originates from the random placement of discrete number of dopants in nanoscale transistors. The number of dopants in a modern nanoscale transistor is so small that these statistically distributed dopants can only be present at certain channel regions of a transistor (see the red solid spots in Figure 12a). In these circumstances, different channel regions of the transistor can have different local V_T, depending on the presence (higher V_T) and absence (lower V_T) of dopants along the 2D surface of a transistor. With the application of small source-drain bias (V_{DS}) and for small V_G (such that only those channel regions, which have no dopant, are conducting), the current conduction from source to drain (I_{DS}) will depend on the connectivity between the low V_T regions. Such connectivity can be simulated by changing the conductances of the 2D channel regions in such a way that the regions having low V_T (or no dopant) have finite conductance and regions having high V_T (or with dopants) have zero conductance (see Figure 12b). Solving such percolative conductance network (using the algorithm of Ref. 26), one can calculate the conductivity of the transistor at small V_{DS} and V_G.

Now, let us consider the effect of single interface defect in the transistor of Figure 12. Similar to the influence of dopant on current conduction, here we also assume the current conduction is suppressed near the interface defect. So, if an interface defect is created in regions away from the percolation path (*e.g.*, within the dashed circle of Figure 12b), then ΔV_T will be very small;

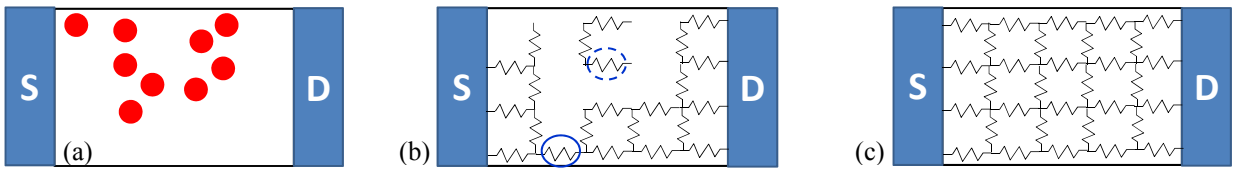

Figure 12: (a) Two-dimensional cross-section of a MOS transistor, showing the placement of dopants with red solid circles. (b) The portion of transistor 2D region (having no dopants) can be connected using a combination of conductances to represent the current conduction at small V_{DS} and V_G. Now, the generation of interface defect in the dashed oval region will correspond to zero ΔV_T, as it does not affect the current conduction; whereas, the generation of interface defect in the solid oval region breaks the percolation path from source to drain, and hence will cause large ΔV_T. (c) The conductance network used for simulating the effect of interface defect on ΔV_T.

because increase in V_T of that region does not affect the current conduction. On the other hand, if the defect is created on the percolation path (*e.g.*, within the solid circle region of Figure 12b), then the current conduction will be severely affected; as a result, ΔV_T will be significantly high. The occurrence of such events (*i.e.*, interface defect being created on top of a percolation path) are rare events and hence, exponentially less likely. Therefore, the distribution of ΔV_T due to a single interface defect has an exponential behavior, as reported in Ref. 22-25. In the following discussion, we confirm the presence of such exponential behavior by performing a generalized percolative conductance network simulation.

3.1 Random Resistive Network Simulation

In this section, we calculate the conductance of transistor region near the substrate/dielectric 2D interface of a transistor by using the conductance network of Figure 12c. The situation represents current conduction at small V_{DS} and small V_G. In such bias condition, the channel regions having dopants and/or interface defects will be devoid of inversion carriers (which will be represented by zero conductance in those regions of Figure 12c) and the remaining channel regions will have finite amount of inversion carriers (which will be represented by conductance in those regions of Figure 12c). So, the conductance in different segments of the 2D surface in Figure 12c will depend on the position of dopants (and/or interface defects) in that region or, in other words, each random placement of dopant (and/or interface defects) removes one conductive region from the network. Therefore, each conductor in Figure 12c represents the conductance of an area of $A_t = \pi r_c^2$, where, the screening radius, $r_c = q^2/4\pi\varepsilon_{Si}kT \sim 4.7$nm (at room temperature) is presumed to be independent of carrier concentration (though, in principle, r_c will reduce at very high carrier concentration [50]).

Here, we choose a 3x8 conductance network for simulating the conduction over a ~1nm thick MOS interfacial region, assuming that such 1nm interfacial layer constitutes the dominant conducting regions at $V_G \sim V_T$ and small V_{DS}. Hence, the active transistor area of the MOS structure will be ~ 0.0027μm^2, corresponding to mean dopants of μ_D~13 (assuming a doping density of 5x10^{18} cm^{-3}), with a statistical spread of $\pm 3\sigma_D$ (assuming Poisson distribution, as used in literature[51]). We calculate the conductance of this network, using the algorithm developed in Ref. 26, by placing specific number of dopants (having any values within ~13±3σ) at random locations. As discussed earlier, we introduce the effect of

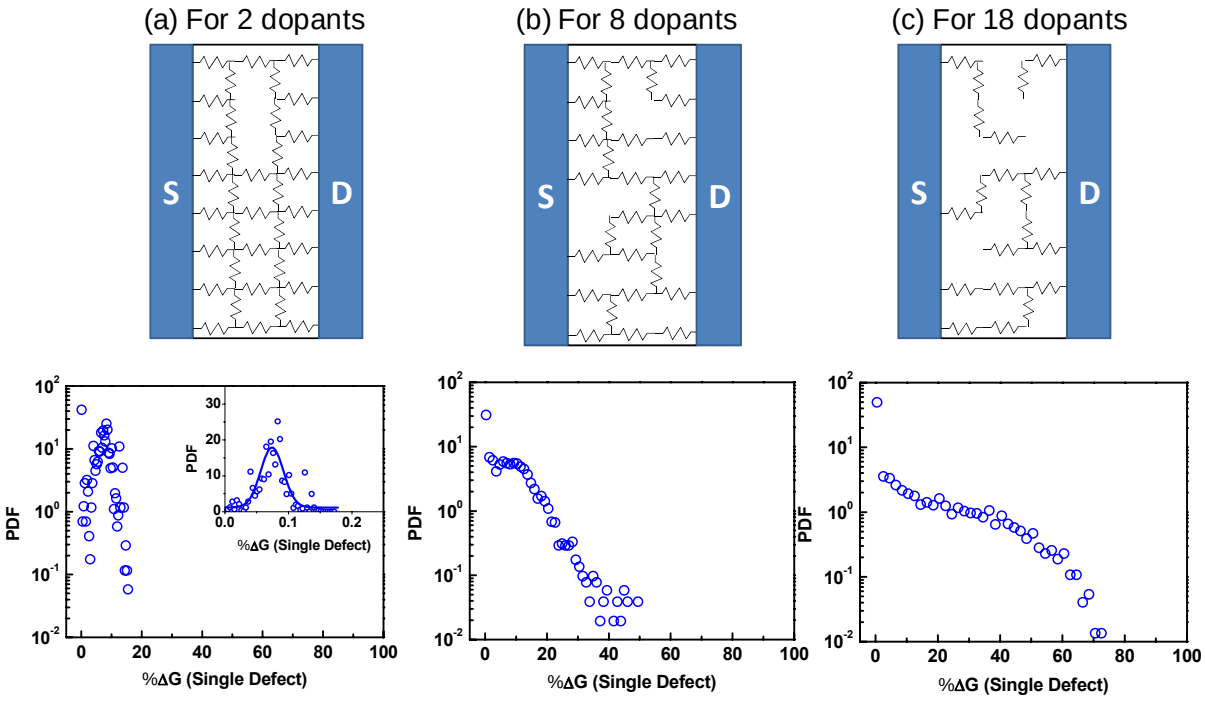

Figure 13: Top: A particular arrangement of conductances for (a) 2 dopants, (b) 8 dopants, and (c) 18 dopants. Bottom: ΔG distribution due to random placement of single interface defect, which has been simulated for 10000 transistors, having (a) 2 dopants, (b) 8 dopants, and (c) 18 dopants.

dopants by reducing the local conductance at ~ $\mu_D \pm 3\sigma_D$ random locations to zero, as shown in Figure 12c. Next, we calculate the effect of single additional interface defect (in terms of change in conductance) by placing the defect at a random location; avoiding the locations occupied by pre-existing dopants (because inversion charge in these doped regions are comparatively small, which reduces the possibility of interface defect creation). The distribution of the change in conductance (ΔG) based on simulation of 10000 configurations (each having different random placement of dopants) is shown in Figure 13. We observe that distribution for ΔG (equivalently, ΔV_T due to single interface defect) is exponential, only if the number of dopants is so large that the transistor is close to percolation. When the number of dopants is reduced (see Figure 13a), change in conductance is small and is described by skewed Gaussian distribution (see inset of Figure 13a). Increasing the number of dopants pushes the channel conductance of the network towards the percolation limit and hence ΔG (or equivalently ΔV_T) begins to increase substantially (Figure 13b,c).

3.2 Effect of Single defect on ΔVT Distribution

For a particular MOS technology, ΔG or ΔV_T distribution due to spatial placement of a single defect will depend on the number of dopants (range of ~ $\mu_D \pm 3\sigma_D$) in a given transistor. Assuming Poisson distribution for the number of dopants in the transistor technology under study (having a mean doping density of $5\text{x}10^{18}$ cm^{-3} and active transistor area of ~ $0.0027\mu\text{m}^2$), in the last section, we have determined ΔG distribution for each dopant configuration (*i.e.*, $\Delta G_{\mu_D\text{-}3\sigma_D}, \ldots \ldots, \Delta G_{\mu_D+3\sigma_D}$). Then, we

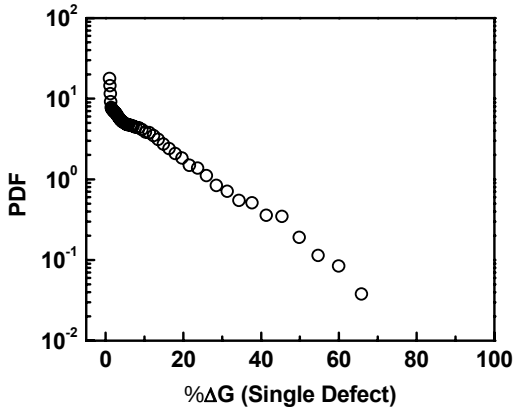

Figure 14: ΔG distribution due to random placement of single interface defect for a transistor technology having a mean doping density of $5\text{x}10^{18}\text{cm}^{-3}$ and an active area of ~ $0.0027\mu\text{m}^2$.

sum up these individual distributions using Poisson statistics and obtain the ΔG distribution for the entire technology. Figure 14 suggests such ΔG distribution (due to single interface defect) to be an exponential, with finite amount of transistors having $\Delta G \sim 0$. Our observation is consistent with the reports in Ref. 22, obtained using 3D drift-diffusion simulation, and in Ref. 23, 25, which is obtained through an equivalent analysis based on SPICE modeling.

4. The Spatio-Temporal Statistics of $\Delta V_T@T_{STS}$

From our analysis in sections 2 and 3, we find that the distribution of $N_{IT}@t_{STS}$ or $P(N_{IT})$ follows a skew-normal distribution of eqn. (17) and distribution of ΔV_T due to single defect or $f_{N_{IT}=1}(\Delta V_T)$ follows an exponential distribution of -

$$f_{N_{IT}=1}(\Delta V_T) = \frac{1}{\eta}\exp\left(-\frac{\Delta V_T}{\eta}\right), \tag{19}$$

along with a certain number of transistors with $\Delta V_T \sim 0$. Since ΔV_T due to subsequent placement of defects is uncorrelated [22], we can follow the procedure of Ref. [23, 25, 52] to determine the spatio-temporal distribution of $\Delta V_T@t_{STS}$. The PDF and CDF of $\Delta V_T@N_{IT}$ can be expressed as –

$$\begin{aligned} f_{N_{IT}}(\Delta V_T) &= \int_0^{\Delta V_T} f_{N_{IT}-1}(\Delta V_T) f_1(\Delta V_T - \Delta V)\, d(\Delta V) \\ &= \frac{\exp(-\Delta V_T/\eta)}{(N_{IT}-1)!}\frac{\Delta V_T{}^{N_{IT}-1}}{\eta^{N_{IT}}}, \end{aligned} \tag{20}$$

$$F_{N_{IT}}(\Delta V_T) = 1 - \frac{\Gamma(N_{IT}, \Delta V_T/\eta)}{(N_{IT}-1)!}. \tag{21}$$

Therefore, the distribution of $\Delta V_T@t_{STS}$ can be expressed as –

$$f(\Delta V_T) = \exp(-\mu_{IT})\left[\begin{array}{l}\delta(\Delta V_T) + \\ \dfrac{d}{dx}\left[\displaystyle\sum_{N_{IT}=1}^{\infty} P(N_{IT}) F_{N_{IT}}(\Delta V_T)\right]\end{array}\right], \tag{22}$$

where the dirac-delta function in equation (22) represents the fraction of devices having zero ΔV_T due to N_{IT}, as observed for a single interface defect in Figure 12. The expression in eqn. (22) matches closely the non-negative $\Delta V_T@t_{STS}$ distribution available in literature[9, 17, 19]. One illustrative example is shown in Figure 15, where one NBTI statistics measurement in Fig. 12 (medium stress data) of Ref. 19 is matched using a variation in fitting parameters η = 4.1mV, μ_{IT} = 9, σ_{IT} = 2.8, and γ_{IT} = 0.1.[53] Such single experimental verification shows that we can capture the general trend. Strictly speaking, however, one should first separate the N_{IT} components of NBTI[12, 29] and then compare the statistical analysis with the experimentally measured N_{IT} statistics.

5. Conclusion

We have performed a MCMC analysis of the R-D system in small transistors and shown that both the $t_{STS}@N_{IT}$ and $N_{IT}@t_{STS}$ distributions follow log-normal behavior. One can readily observe such log-normal distribution for the $t_{STS}@N_{IT}$ distribution, which is cut-off by the sampling time at lower end and simulation length (or equivalently measurement window) at the higher end. However, due to the constraints of $N_{IT} > 0$ and smaller (log-scale) standard deviation, log-normal behavior is seldom seen in $N_{IT}@t_{STS}$ distribution. The distribution is either skewed towards the higher N_{IT} side (from constraints of $N_{IT} > 0$) or approaches a Gaussian distribution (due to smaller log-scale standard deviation). Such behavior is universally observed in the R-D system, irrespective of the diffusing species being H or H_2. Moreover, our analysis suggests that $N_{IT}@t_{STS}$ distribution should always be non-negative, unless there are pre-existing N_{IT} in certain statistically rare transistors. Later, we describe the effect of spatial distribution of $N_{IT}@t_{STS}$ in a percolative network and show that the distribution of ΔV_T for single interface defect is exponential, with finite number of transistors having zero ΔV_T. Finally, utilizing these two distributions for $N_{IT}@t_{STS}$ and $\Delta V_T@N_{IT}$, we obtain an expression for $\Delta V_T@t_{STS}$ statistics, which nicely captures the experimental results. The developed framework for estimating $\Delta V_T@t_{STS}$ statistics should be useful in analyzing NBTI distribution for transistors having dominant interface defect generation or for the cases of AC NBTI degradation, where the parasitic hole trapping components (a component of DC NBTI) becomes negligibly small and shift in threshold voltage reflects the sole contribution from interface trap generation.

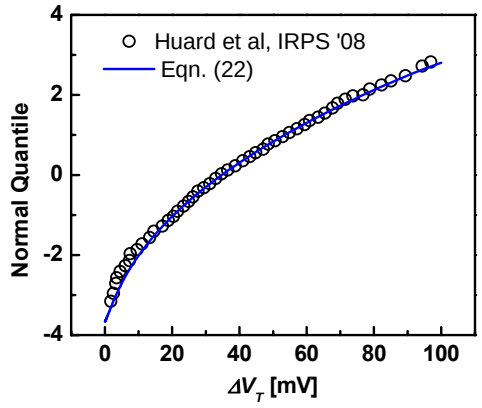

Figure 15: Eqn. (22) *is consistent with experimentally measured* $\Delta V_T@t_{STS}$ distribution of Ref. 19.

Acknowledgements

We acknowledge Dhanya Varghese for developing the random percolative network code used in section 3. We gratefully acknowledge financial support from Intel Corporation though the Intel Foundation PhD Fellowship (2009-2010) and computational resources from Network of Computational Nanotechnology.

References

1. D. K. Schroder and J. A. Babcock, Journal of Applied Physics **94** (1), 1-18 (2003).
2. M. A. Alam and S. Mahapatra, Microelectronics Reliability **45** (1), 71-81 (2005).
3. V. Huard, M. Denais and C. Parthasarathy, Microelectronics Reliability **46** (1), 1-23 (2006).
4. A. E. Islam, H. Kufluoglu, D. Varghese, S. Mahapatra and M. A. Alam, Ieee Transactions on Electron Devices **54** (9), 2143-2154 (2007).
5. T. Grasser, W. Gos, V. Sverdlov and B. Kaczer, presented at the IEEE International Reliability Physics Symposium, 2007 (unpublished).
6. M. F. Li, D. M. Huang, C. Shen, T. Yang, W. J. Liu and Z. Y. Liu, Ieee Transactions on Device and Materials Reliability **8** (1), 62-71 (2008).
7. S. Mahapatra, K. Ahmed, D. Varghese, A. E. Islam, G. Gupta, L. Madhav, D. Saha and M. A. Alam, presented at the IEEE International Reliability Physics Symposium, 2007 (unpublished).
8. Y. Mitani, H. Satake and A. Toriumi, Ieee Transactions on Device and Materials Reliability **8** (1), 6-13 (2008).

9. S. Pae, J. Maiz, C. Prasad and B. Woolery, Ieee Transactions on Device and Materials Reliability **8** (3), 519-525 (2008).

10. K. Bernstein, D. J. Frank, A. E. Gattiker, W. Haensch, B. L. Ji, S. R. Nassif, E. J. Nowak, D. J. Pearson and N. J. Rohrer, IBM Journal of Research and Development **50** (4-5), 433-449 (2006).

11. G. LaRosa, in *Reliability Wearout Mechanisms in Advanced Cmos Technologies* (John Wiley & Sons Inc, 2009), pp. 331-440.

12. A. E. Islam, S. Mahapatra, S. Deora, V. D. Maheta and M. A. Alam, presented at the International Electron Devices Meeting (IEDM) Technical Digest, 2009 (unpublished).

13. J. P. Campbell, P. M. Lenahan, A. T. Krishnan and S. Krishnan, IEEE International Reliability Physics Symposium, 503-510 (2007).

14. S. E. Rauch, Ieee Transactions on Device and Materials Reliability **2** (4), 89-93 (2002).

15. M. Agostinelli, S. Pae, W. Yang, C. Prasad, D. Kenckel, S. Ramey, E. Snyder, S. Kashyap and M. Jones, IEEE International Reliability Physics Symposium, 529-532 (2005).

16. G. La Rosa, W. L. Ng, S. Rauch, R. Wong and J. Sudijono, IEEE International Reliability Physics Symposium, 274-282 (2006).

17. S. E. Rauch, Ieee Transactions on Device and Materials Reliability **7** (4), 524-530 (2007).

18. K. Kang, S. P. Park, K. Roy and M. A. Alam, presented at the IEEE/ACM International Conference on Computer-Aided Design, 2007 (unpublished).

19. V. Huard, C. Parthasarathy, C. Guerin, T. Valentin, E. Pion, M. Mammasse, N. Planes and L. Camus, IEEE International Reliability Physics Symposium, 289-300 (2008).

20. B. Vaidyanathan, A. S. Oates, Y. Xie and Y. Wang, ISQED: International Symposium on Quality Electronic Design, 13-18 (2009).

21. T. Fischer, E. Amirante, P. Huber, K. Hofmann, M. Ostermayr and D. Schmitt-Landsiedel, Solid-State Electronics **53** (7), 773-778 (2009).

22. A. Ghetti, C. M. Compagnoni, A. S. Spinelli and A. Visconti, Ieee Transactions on Electron Devices **56** (8), 1746-1752 (2009).

23. B. Kaczer, P. J. Roussel, T. Grasser and G. Groeseneken, Ieee Electron Device Letters **31** (5), 411-413 (2010).

24. M. F. Bukhori, S. Roy and A. Asenov, Ieee Transactions on Electron Devices **57** (4), 795-803 (2010).

25. B. Kaczer, T. Grasser, P. J. Roussel, J. Franco, R. Degraeve, L.-A. Ragnarsson, E. Simoen, G. Groeseneken and H. Reisinger, presented at the IEEE International Reliability Physics Symposium, 2010 (unpublished).

26. D. J. Frank and C. J. Lobb, Physical Review B **37** (1), 302-307 (1988).

27. S. Mahapatra, V. D. Maheta, S. Deora, E. N. Kumar, S. Purawat, C. Olsen, K. Ahmed, A. E. Islam and M. A. Alam, ECS Transactions **19** (2), 243-263 (2009).

28. S. Deora, V. D. Maheta, A. E. Islam, M. A. Alam and S. Mahapatra, Ieee Electron Device Letters **30** (9), 978-980 (2009).

29. S. Mahapatra, V. D. Maheta, A. E. Islam and M. A. Alam, Ieee Transactions on Electron Devices **56** (2), 236-242 (2009).

30. J. H. Lee and A. S. Oates, Ieee Transactions on Device and Materials Reliability **10** (2), 174-181 (2010).

31. S. Chakravarthi, A. T. Krishnan, V. Reddy and S. Krishnan, Microelectronics Reliability **47** (6), 863-872 (2007).

32. W. P. Wang, V. Reddy, A. T. Krishnan, R. Vattikonda, S. Krishnan and Y. Cao, Ieee Transactions on Device and Materials Reliability **7** (4), 509-517 (2007).

33. S. V. Kumar, C. H. Kim and S. S. Sapatnekar, Ieee Transactions on Device and Materials Reliability **9** (4), 537-556 (2009).

34. T. Grasser, B. Kaczer, W. Goes, T. Aichinger, P. Hehenberger and M. Nelhiebel, IEEE International Reliability Physics Symposium, 33-44 (2009).

35. T. Grasser, B. Kaczer and W. Goes, presented at the IEEE International Reliability Physics Symposium, 2008 (unpublished).

36. A. E. Islam and M. A. Alam, in *unpublished results*.

37. V. Huard, presented at the IEEE International Reliability Physics Symposium, 2010 (unpublished).

38. P. R. Nair and M. A. Alam, Applied Physics Letters **88** (23), - (2006).

39. A. Hassibi, S. Zahedi, R. Navid, R. W. Dutton and T. H. Lee, Journal of Applied Physics **97** (8), - (2005).

40. B. Ray, P. R. Nair, R. E. Garcia and M. A. Alam, presented at the International Electron Devices Meeting (IEDM) Technical Digest, 2009 (unpublished).

41. B. A. Grzybowski, K. J. M. Bishop, C. J. Campbell, M. Fialkowski and S. K. Smoukov, Soft Matter **1** (2), 114-128 (2005).

42. J. Hattne, D. Fange and J. Elf, Bioinformatics **21** (12), 2923-2924 (2005).

43. W. H. Press, *Numerical recipes : the art of scientific computing*, 3rd ed. (Cambridge University Press, Cambridge, UK ; New York, 2007).

44. H. Kufluoglu and M. A. Alam, Ieee Transactions on Electron Devices **54** (5), 1101-1107 (2007).

45. H. S. Wilf, *Generatingfunctionology*, 2nd ed. (Academic Press, Boston, 1994).

46. K. W. Kehr, K. Mussawisade and T. Wichmann, Anomalous Diffusion: From Basics to Applications **519**, 35-44 (1999).

47. K. P. N. Murthy and K. W. Kehr, Physical Review A **40** (4), 2082-2087 (1989).

48. B. J. Zwolinski, H. Eyring and C. E. Reese, Journal of Physical and Colloid Chemistry **53** (9), 1426-1453 (1949).

49. A. Azzalini, Scandinavian Journal of Statistics **32** (2), 159-188 (2005).

50. N. W. Ashcroft and N. D. Mermin, *Solid state physics*. (Holt, New York,, 1976).

51. A. Asenov, Ieee Transactions on Electron Devices **45** (12), 2505-2513 (1998).

52. K. Takeuchi, T. Nagumo, S. Yokogawa, K. Imai and Y. Hayashi, presented at the Symposium on VLSI Technology, 2009 (unpublished).

53. A fitting of the stress time dependent experiments, using eqn. (22) suggests an increase in σ_{IT} with μ_{IT}, as a function of stress time (see supplementary figure). Therefore, our analysis consistently predicts an increase in the variance of ΔV_T with $<\Delta V_T>$, regularly reported in NBTI literature[9, 14, 17, 19].